ChemPhysChem

Research Article
doi.org/10.1002/cphc.202400222

Chemistry Europe
European Chemical Societies Publishing

www.chemphyschem.org

Vibrational Features of Oxyamines: A Comparative Study of *N,N*-Diethylhydroxylamine and *N,N*-Diethylacetyloxyamine

Emanuele Pizzano,[a, b] Filippo Baroncelli,[a] Sonia Melandri,[a, c, d] Luca Evangelisti,[c, d, e] Marcello Ricci,[b] Marzia Mazzacurati,[b] Matteo Pori,[b] Armida Torreggiani,[f] and Assimo Maris*[a, c]

The ability of oxyamines to undergo homolytic cleavage of the O–C bond, leading to the formation of stable radicals, is widely used in polymerization processes and to prevent oxidative stress in materials. We present a mid and near-infrared spectroscopy study on two model compounds, *N,N*-diethylhydroxyloxyamine ($C_4H_{11}NO$) and its acetyl derivative *N,N*-diethylacetyloxyamine ($C_6H_{13}NO_2$) in the liquid phase. The analysis of the spectra is based on a complete exploration of the conformational space, coupled to harmonic and anharmonic calculations performed using the generalized second-order vibrational perturbation theory (GVPT2) formalism at the B3LYP–D3(BJ)/Def2-TZVP level of calculation and potential energy distribution analysis. In the most stable species out of 25, the three amine chains present an all-*anti* arrangement, with the carbonyl oxygen atom pointing towards the nitrogen lone pair. The simulated spectra are in overall good agreement with the experimental ones, and suitable for the assignment of the main observed bands. Furthermore, similarities and divergences between the two molecules are discussed.

Introduction

Spectroscopy in the mid-infrared (MIR, 400–4000 cm^{-1}) and near-infrared (NIR, 4000–12500 cm^{-1}) ranges allows us to probe the vibrational spectra of molecules. In particular, the lower frequency region is characterised by fundamental vibrational modes, while the higher frequency region is characterised by overtones and combination bands involving the X–H stretching motions, where X is a heavy atom (i.e. X=C, N, O).[1]

The MIR technique is more sensitive and the spectrum is simpler to understand. On the other hand, NIR spectroscopy benefits from simple analysis setups, with glass cuvettes being sufficient to perform the measurements and it is suitable for monitoring online processes. However, the interpretation of the spectral features becomes challenging and multivariate statistical methods must be applied to extract information.

The accuracy and robustness of multivariate models hinge on the quality of the input spectra as well as a series of choices done during the construction of the models themselves. By providing a more realistic representation of molecular vibrations, quantum mechanical simulations contribute to the reliability of models for quantitative assessment and reduce the risk of over-fitting.[2]

However, predicting vibrational spectra including overtones and combination bands still represents a challenge and the study of small model systems constitutes an important test bench for calculations. For this reason, here we present an experimental and quantum mechanical comparative study on *N,N*-diethylhydroxylamine (DEHA for short) and *N,N*-diethylacetyloxyamine (DEAcA for short, see Figure 1) two small ternary organic compounds characterized by relatively high molecular flexibility.

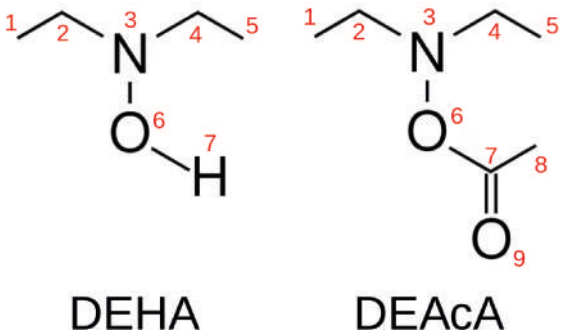

Figure 1. Sketch and numbering of the skeletal atoms of *N,N*-diethylhyroxylamine ($C_4H_{11}NO$) and its acetyl derivative *N,N*-diethylacetyloxyamine ($C_6H_{13}NO_2$).

[a] *E. Pizzano,+ F. Baroncelli,+ Prof. Dr. S. Melandri, Prof. Dr. A. Maris*
Department of Chemistry G. Ciamician, University of Bologna, Bologna, Italy
E-mail: assimo.maris@unibo.it

[b] *E. Pizzano,+ M. Ricci, Dr. M. Mazzacurati, Dr. M. Pori*
BASF Italia S.p.A., Pontecchio Marconi (BO), Italy

[c] *Prof. Dr. S. Melandri, Prof. Dr. L. Evangelisti, Prof. Dr. A. Maris*
Interdepartmental Centre for Industrial Aerospace Research (CIRI Aerospace), University of Bologna, Forlì, Italy

[d] *Prof. Dr. S. Melandri, Prof. Dr. L. Evangelisti*
Interdepartmental Centre for Industrial Agrifood Research (CIRI Agrifood), University of Bologna, Cesena, Italy

[e] *Prof. Dr. L. Evangelisti*
Department of Chemistry G. Ciamician - Campus of Ravenna, University of Bologna, Ravenna, Italy

[f] *Dr. A. Torreggiani*
Istituto I.S.O.F., Consiglio Nazionale delle Ricerche, Bologna, Italy

Supporting information for this article is available on the WWW under https://doi.org/10.1002/cphc.202400222

Oxyamines are characterized by the N–O bond. They serve as intermediates for synthesizing different organic compounds, where the reversible homolytic cleavage of the C-ON bond is a crucial step for creating stable nitroxides. The stability of the NO frame is dependent on the delocalization of the unpaired electron, creating a two-centre three-electron N–O bond. The molecular structure can influence this stability, opening up numerous potential applications. Among them, nitroxide-mediated polymerization (NMP) is used to generate complex macromolecular architectures with well-controlled stereochemistry, high chain end homogeneity and a very low polymer dispersity without needing transition metal complexes.[3,4] Nitroxides are also used as intermediates in the Denisov cycle,[5] a catalytic process occurring in plastic materials added with hindered amine light stabilizers (HALS) in order to prevent their photodegradation. Moreover, several studies explore oxyamines as precursors of radicals that can serve as therapeutic[6] and theranostic agents.[7] In addition, oxyamines are involved in the synthesis of bifunctional linkers applied to glycoconjugates with high stability towards hydrolysis even with various pH conditions.[8] N–O bond-containing oxidants, including DEAcA, can be used instead of silver or copper salts for mild and efficient syntheses of isocoumarins, isoquinolines, isoquinolinone, and styrenes via C–H activation catalyzed by pentamethylcyclopentadienyl complexes of Co(III), Rh(III) and Ir(III).[9] Recently, magnetic iron oxide nanoparticles covalently grafted with a thermosensitive radical initiator alkoxyamine have been synthesized and characterized. They exhibit a rapid heating of their surface under the action of an alternate current magnetic field, inducing the homolysis of the C–ON bond and then the oxygen-independent formation of radicals.[10]

The interest in oxyamines revolves essentially around the peculiar properties of the N–O bond that are affected by the intra- and inter-molecular interactions, which also determine the molecular geometry. Conducting a systematic study of various oxyamines through theoretical and spectroscopic methods would provide valuable insights into the fundamental properties of this class of compounds. For this reason, we recently reported detailed studies on DEHA and its 1:1 water complex. We have found that in the gas phase, the preferred arrangement of the alkyl chains is *anti* and the hydroxyl hydrogen atom is directed toward the nitrogen lone pair.[11,12] Upon ionization, a strong structural rearrangement takes place changing the amine nitrogen to N-oxoammonium.[11] Microsolvation with a water molecule leads to the formation of a 5-member ring closed by two hydrogen bonds: HOH·NOH and H_2O·HON.[13] Rather surprisingly, the interaction involving nitrogen is stronger than the one involving oxygen. As a following step, we present the study of DEAcA, the acetyl-substituted compound, highlighting the effect of replacing the hydroxyl hydrogen atom with an organic group by the analysis of its MIR and NIR spectra.

Synthesis and Thermal Stability of DEAcA

Zimmer made the first tentative synthesis of DEAcA by adding DEHA to a solution of chloroform and ethenone, obtaining a moderately pure product.[14] Huisgen and Beyerlein proposed another synthesis pathway by stirring DEHA with acetic anhydride.[15] Following the same approach Perrin et al. could obtain DEAcA with 22% yield.[16] We based the synthesis of DEAcA methodology reported for acylation of hydroxylamine derivatives with benzoyl chloride.[17] A similar approach was used by Liu et al. to synthesize DEAcA.[9] The overall reaction, conducted at room temperature, can be described as:

$$Et_2NOH + MeC(O)Cl \xrightarrow[CH_2Cl_2]{NMe_3} Et_2NOC(O)Me + HCl \quad (1)$$

The purity of DEAcA was tested with both gas-chromatography electron ionization mass spectrometry (GC/EI-MS) and nuclear magnetic resonance (NMR) spectroscopy, while its thermal stability was tested by differential scanning calorimetry (DSC) preparing the sample under a nitrogen atmosphere and keeping it in a high-pressure gold-plated crucible. The DSC curve in Figure 2, shows a very intense peak centred at 183.45 °C (456.60 K), corresponding to an exothermic process whose released energy is 1323.74 J/g (173.64 kJ·mol^{-1}).

The shape of the peak suggests the detection of an intense autocatalytic phenomenon that starts to produce energy already at 126.41 °C (399.56 K). A possible reaction could be either an inter- or intra-molecular decarboxylation of DEAcA leading to the formation of *N*,*N*-diethylmethylamine, i.e.:

$$Et_2NOC(O)Me \rightarrow Et_2NMe + CO_2 + Q \quad (2)$$

Actually, in agreement with density functional theory (DFT) calculations (B3LYP–D3(BJ)/Def2-TZVP), this reaction is highly exothermic and the released energy is estimated to be 151 kJ·mol^{-1}, in rough agreement with the experimental findings. We suggest handling DEAcA on a milligram scale, at a low temperature, diluted and storing it very cold.

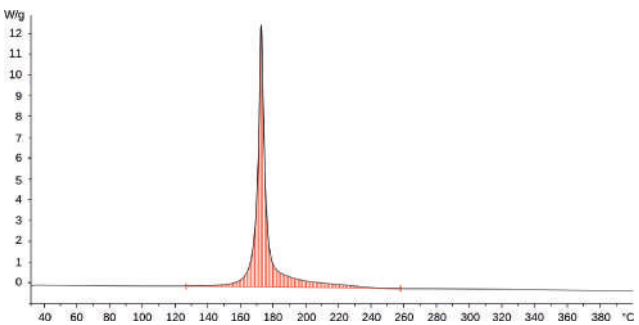

Figure 2. DSC test on *N*,*N*-diethylacetyloxyamine. A heating ramp from 303 K to 673 K at 4 K/min was applied. The source temperature values are reported in the abscissa.

Conformational Space

DEAcA is a flexible molecule and its conformations are defined by the orientation of the ethyl chains (α and β = CCNC dihedral angles), the acetoxy group (γ = CONL, where "L" is the bisector line of the CNC bond angle) and the acetyl group (δ = OCON) as shown in Figure 3.

The values of the skeletal torsion angles are summarized in a four-letter code describing the values of the α, β, γ and δ sequence according to the *sin* ($\simeq 0^\circ$, s for short), *anti* ($\simeq 180^\circ$, a), *gauche* ($\simeq 60^\circ$, g) or *gauche'* ($\simeq 300^\circ$, g') labelling. It is worth noting that α, β and δ define the orientation of the side chains whereas γ is kind of an internal dihedral angle. For this reason, it is described with a capital letter.

A systematic exploration of the conformational space, performed at the B3LYP–D3(BJ)/Def2-TZVP level of calculation, allowed the identification of 25 non-equivalent conformers, aaAs being the global minimum. 14 conformers have the acetyl group oriented toward the nitrogen lone pair ($\gamma \simeq 180^\circ$, *ANTI*) and their relative energy is between 0 and 1788 cm^{-1}. The remaining 11 conformers have the acetyl group oriented toward the ethyl chains ($\gamma \simeq 0^\circ$, *SYN*) and their relative energy is between 958 and 5338 cm^{-1}. Depending on the mutual orientation of the ethyl chains (α and β), six different arrangements can be recognized: aa, ga and equivalent ag', ag and equivalent g'a, gg and equivalent g'g', gg' and g'g where the *anti* orientation is more stable than the *gauche* ones. In gg' and g'g arrangements the terminal methyl groups are faced each other, therefore, in order to reduce the steric hindrance, the α and β dihedral angles assume non-symmetric values, leading to the formation of two equivalent conformers (except g'gAa). The carbonyl group is found to be *syn* or *anti* with respect to the nitrogen atom. The former arrangement is the most stable and the energy difference is 200–300 cm^{-1} for the *ANTI* conformers and about 3000 cm^{-1} for the *SYN* conformers, due to steric hindrance between the acetyl methyl group and the ethyl chains. In both ggAs and gg'As the δ angle can assume two different values leading to two non-equivalent minima in the conformational energy surface, identified as s' and s", respectively. The molecular properties of conformers (symmetry group representation, number of equivalent species, relative energies and abundances) are given in Table 1 while their structures are reported in Tables S1-S25 of the Supporting Information.

By comparing the structures of DEAcA and DEHA[11] it is evident that the global minima have the same arrangement of the common molecular frame. The conformational space of DEHA is defined by only three degrees of freedom: α and β which describe the orientation of the ethyl chains as for DEAcA, and γ which describes the hydroxyl position. Hence a tree-letter code can be used to describe the 12 possible conformers. In particular, the aaA species is the most stable and similarly the global minimum of DEAcA is aaAs. However, another related species exists, where the acetyl frame has a different orientation, that is aaAa. To visualize the relation between the DEHA and DEAcA conformers sharing the same values of α, β and γ, a relative energy correlation diagram is given in Figure 4.

The most stable structures were further optimized using both a different triple-ζ basis set (aug-cc-pVTZ) and a different density functional (M06-2X), as well as the *ab initio* MP2 approach. The obtained relative electronic energy and relative zero-point energy values are compared in Table 2. Despite these values varying up to 165 cm^{-1}, some trends can be recognized: aaA-DEHA and aaAs-DEAcA are the global minima, followed by gaA-DEHA, aaAa-DEAcA and gaAs-DEAcA (the latter ones being almost isoenergetic), then there are agA-DEHA and agAs and finally gaAa-DEAcA. It is worth noting that including

Table 1. Properties of the conformers of DEAcA obtained at the B3LYP–D3(BJ)/Def2-TZVP level of calculation: symmetry group representation (Γ), number of equivalent species (*deg.*), theoretical relative energy (ΔE_e and ΔE_0/cm^{-1}), relative abundance at 298.15 K.

Conformer	Γ	*deg.*	ΔE_e	ΔE_0	N_i/N_1
aaAs	C_s	1	0	0	1
gaAs/ag'As	C_1	2	260	309	$4.51{\cdot}10^{-1}$
agAs/g'aAs	C_1	2	447	493	$1.85{\cdot}10^{-1}$
ggAs'/g'g'As'	C_1	2	720	826	$3.71{\cdot}10^{-2}$
ggAs"/g'g'As"	C_1	2	730	833	$3.59{\cdot}10^{-2}$
gg'As'	C_1	2	1098	1185	$6.56{\cdot}10^{-3}$
gg'As"	C_1	2	1201	1281	$4.13{\cdot}10^{-3}$
g'gAs	C_1	2	1549	1665	$6.47{\cdot}10^{-4}$
aaAa	C_s	1	220	370	$1.67{\cdot}10^{-1}$
gaAa/ag'Aa	C_1	2	551	670	$7.88{\cdot}10^{-2}$
agAa/g'aAa	C_1	2	673	811	$3.99{\cdot}10^{-2}$
ggAa/g'g'Aa	C_1	2	961	1126	$8.72{\cdot}10^{-3}$
gg'Aa	C_1	2	1552	1632	$7.60{\cdot}10^{-4}$
g'gAa	C_s	1	1788	1898	$1.05{\cdot}10^{-4}$
aaSs	C_s	1	958	994	$8.26{\cdot}10^{-3}$
gaSs/ag'Ss	C_1	2	1166	1207	$5.91{\cdot}10^{-3}$
agSs/g'aSs	C_1	2	1906	1973	$1.46{\cdot}10^{-4}$
ggSs/g'g'Ss	C_1	2	2128	2190	$5.13{\cdot}10^{-5}$
gg'Ss	C_1	2	1782	1859	$2.54{\cdot}10^{-4}$
g'gSs	C_1	2	3334	3377	$1.67{\cdot}10^{-7}$
aaSa	C_s	1	4123	4192	$1.64{\cdot}10^{-9}$
gaSa/ag'Sa	C_1	2	4319	4363	$1.43{\cdot}10^{-9}$
agSa/g'aSa	C_1	2	5189	5311	$1.5{\cdot}10^{-11}$
ggSa/g'g'Sa	C_1	2	5338	5441	$7.9{\cdot}10^{-12}$
gg'Sa	C_1	2	4724	4753	$2.2{\cdot}10^{-10}$

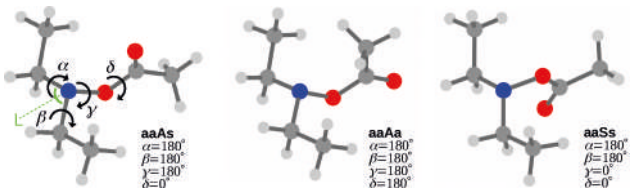

Figure 3. Structure of three conformers of DEAcA showing the bisector of the CNC bond angle (L), and the dihedral angles (α, β, γ and δ). The aaAs conformer is the global minimum.

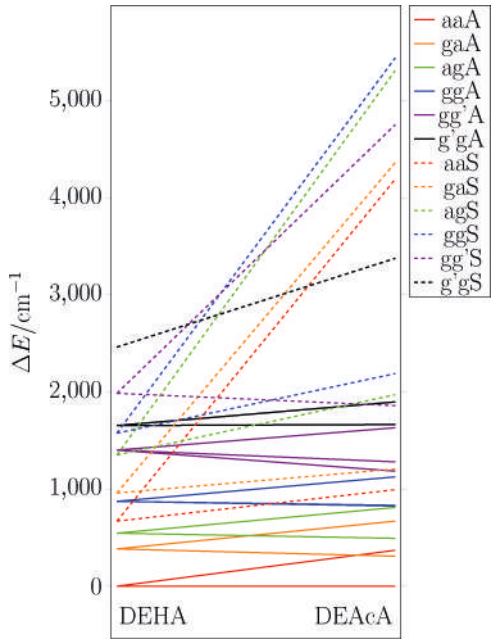

Figure 4. Correlation energy diagram between the DEHA and DEAcA showing the effect of the acetyl group substituent and its orientation on the relative stability of the conformers (zero-point corrected energy values at the B3LYP–D3(BJ)/Def2-TZVP level of calculation).

Table 2. Theoretical relative energy values ($\Delta E_e/\Delta E_0$ in cm^{-1}) of the most stable conformers of DEAcA (with respect to the global minimum, aaAs) and DEHA (with respect to the global minimum, aaA) obtained at different levels of calculation.

DEAcA	aaAa	gaAs	gaAa	agAs
MP2				
Def2-TZVP	325/471	302/357	710/818	542/611
aug-cc-pVTZ	218/377	298/378	639/762	576/656
M06-2X				
Def2-TZVP	226/399	308/371	665/786	437/491
aug-cc-pVTZ	196/369	296/441	641/771	447/515
B3LYP–D3(BJ)				
Def2-TZVP	220/370	260/309	551/670	447/493
aug-cc-pVTZ	211/365	262/318	546/670	466/519
DEHA		gaA		agA
MP2				
Def2-TZVP		354/390		591/592
aug-cc-pVTZ		361/359		556/585
M06-2X				
Def2-TZVP		413/401		456/466
aug-cc-pVTZ		386/359		455/457
B3LYP–D3(BJ)				
Def2-TZVP		387/384		527/546
aug-cc-pVTZ		337/341		501/530

the zero-point energy correction increases the relative energy values of all considered DEAcA conformers. As anticipated, aaAa-DEAcA and gaAs-DEAcA are very close in energy and, depending on the kind of calculation, the energy hierarchy can change. In any case, when considering the degeneracy factor, gaAs-DEAcA is the most abundant species at room temperature after the global minimum (about 1/3) whereas aaAa-DEAcA and agAs-DEAcA are almost equally abundant (about 1/7). Similarly, the abundancies of gaA-DEHA and agA-DEHA are about 1/3 and 1/7 to the all-*anti* form.

Finally, as regards the rotation of the methyl groups (α and β angles) it was estimated that the conversion barriers from gaA-DEHA and agA-DEHA to aaA-DEHA are equal or greater to about 11 $kJ\,mol^{-1}$, at the B3LYP–D3(BJ)/Def2-TZVP level of calculation.[11] Similar behaviour is expected for DEAcA.

MIR Spectroscopy

The experimental MIR spectra of liquid DEAcA and DEHA in the 400–3700 cm^{-1} spectral region are reported in Figure 5, where they are compared to the simulated ones based on the harmonic frequencies at the B3LYP–D3(BJ)/Def2-TZVP level of calculation. The recorded spectrum of DEHA well compares with those reported in the NIST[18] and Sigma-Aldrich® datasets.

For each species, only the most stable conformers were considered, namely aaAs, aaAa, gaAs and agAs for DEAcA and aaA, gaA and agA for DEHA, weighting the particular contributions according to the abundance ratios estimated in the previous section. An overall agreement between experimental and theoretical data is found and with the support of potential energy distribution (PED) analysis, the assignment of the main peaks can be attempted. The theoretical normal modes of the global minima of DEHA and DEAcA were decomposed in a linear combination of local modes by PED, which are classified as stretching (ν), bending (δ) and linear (τ) or tetrahedral (γ) torsion motions, involving 2, 3 or 4 atoms respectively.

A broad band between 3000 and 3500 cm^{-1} characterises the spectrum of DEHA. This band can be ascribed to the stretching motion of the hydroxyl group which, being polar in the liquid phase, is strongly affected by the intermolecular interactions which contribute to the broadening of the band. Actually, the predicted value for the isolated molecule lies at 3649 cm^{-1}. The 2800–3000 cm^{-1} interval comprehends the C–H stretching modes. According to the theoretical prediction, the peaks' intensity is mainly due to the ethyl chains rather than the acetyl group, and, coherently, the spectra for the two molecules are quite similar.

In the lower frequency region, the spectrum of DEAcA is dominated by the features of the acetyl group. The observed carbonyl group stretching of DEAcA is at 1760 cm^{-1}, lower than that measured in 1,4-dioxane solution (1766 cm^{-1}).[19] The observed value is blue-shifted with respect to that of esters, which can be considered analogous compounds where the secondary amine is replaced by an alkyl group. Indeed, the peak of methyl acetate, obtained by Raman liquid measurements, lies at 1743 cm^{-1}, respectively.[20] Two weak features at

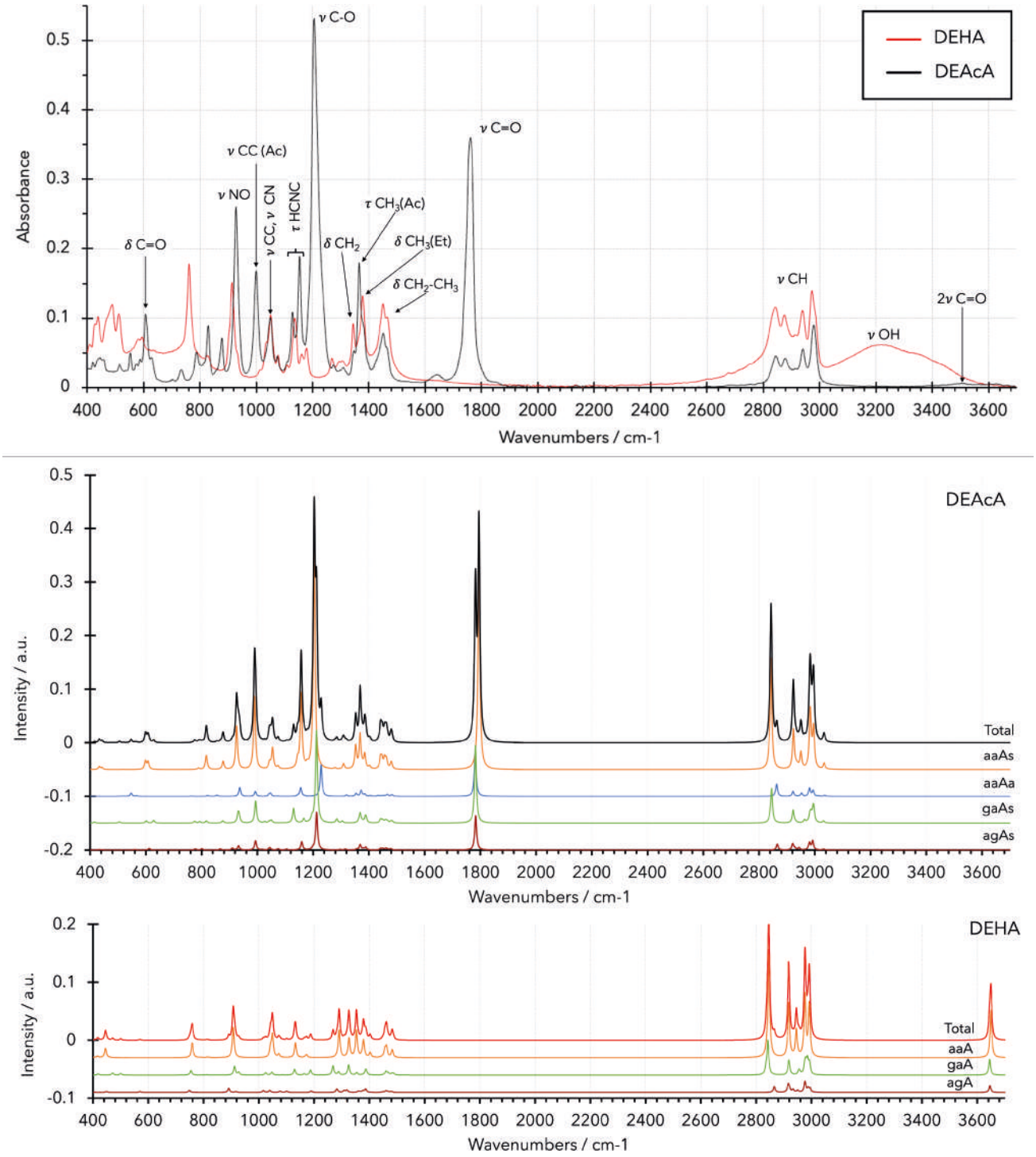

Figure 5. Experimental (top panel) and simulated (bottom panels) MIR spectra of DEAcA (black traces) and DEHA (red traces) collected at room temperature. The simulated spectra are obtained at the B3LYP–D3(BJ)/Def2-TZVP level of calculation considering the contribution of the most abundant conformers and using scaling factors 0.98 or 0.96 for wavenumbers below or above 2000 cm^{-1}, respectively.

3512 and 3628 cm^{-1} are also observed in the spectrum of DEAcA. The first one is compatible with the first overtone of the carbonyl group stretching, whereas the second one should involve the combination of three quanta. The most intense peak of DEAcA lies at 1205 cm^{-1} and is assigned to the stretching motion of the C–O bond. This value is red-shifted to that of methylacetate (1242 cm^{-1}),[20] suggesting that the C–O bond is weaker in acetoxyamines than in acetates. Peaks related to the acetyl frame are also the C–C stretching at 999 cm^{-1} and the carboxyl bending at 606 cm^{-1}. Consistently, all these features are absent in the spectrum of DEHA.

On the contrary, the N–O stretching is visible in both spectra, at 928 cm^{-1} and 913 cm^{-1} for DEAcA and DEHA, respectively, the latter value being close to that of hydroxylamine in solid state, 912 cm^{-1}.[21] The experimental 15 cm^{-1} blue shift observed upon acetylation is consistent with the calculated one (18 cm^{-1}). The PED analysis highlights that in DEHA the contribution of the NO stretching to the involved normal mode is dominant (47%) whereas it lowers in DEAcA (25%), where it is combined with the C–O (26%) and C–C (19%) stretching motions of the acetyl frame. Notably, in the case of DEHA the N–O stretching (42%) combined with the N–C stretching motions (14% each) is responsible for the intense peak at 761 cm^{-1}. The corresponding feature for DEAcA could be identified as the weak peak at 787 cm^{-1}, which is a combination of the N–O (20%) stretching and NOC bending (10%) motions. The C–C and C–N stretching modes concerning the diethylamine frame are centred around 1050 cm^{-1}.

Bending and torsion modes involving the CH groups can be observed in the 1120–1450 cm^{-1} range. In particular, the peaks of DEAcA at 1152 and 1128 cm^{-1}, involving the HCNC frame can be ascribed to the conformers which differ for the orientation of one of the ethyl chains: aaAs and aaAa for the higher energy peak a gaAs and gaAa for the lower energy one. Finally, in the fingerprint region, the bending and torsion motions of the molecular skeleton are observed.

Detailed data are given in the Supporting Information: the fundamental wavenumbers and intensities calculated for each conformer are listed in Tables S26-S35, PED's local modes are reported in Tables S36-S37, the main contributions (>10%) of different local coordinates to the normal vibration modes are summarized Tables S38-S39, and the list of the measured peaks' wavenumber and absorbance is available in Tables S40-S41.

NIR Spectroscopy

The experimental NIR spectra of liquid DEHA and DEAcA in the 4500–9500 cm^{-1} range, recorded at different working temperatures (60-100 °C) are compared in Figure 6, and the list of the measured peak wavenumbers and absorbances is available in Tables S43-S44. Comparison of the gas and liquid phase NIR spectra of DEAcA, reported in the Supporting Information, evidences a similar profile.

The simulated spectrum of DEAcA based on the anharmonic vibrational frequencies calculated for the most stable conformer is also reported in the same figure together with a heatmap representation of the contribution of the two- and three-quanta vibrational transitions, as first proposed by Beć *et al.*[22] Theoretical binary and ternary combination bands, first and second overtones account 43.3%, 45.9%, 9.5% and 1.3% of the overall spectral intensity, respectively. As regards DEHA we assume the assignment relative to the gas phase spectrum as a starting point.[11]

Comparison between the DEHA and DEAcA spectra shows that the spectral regions characterized by the CH motions are quite similar. In particular, the two quanta transitions involving the CH stretching motions (5500–6200 cm^{-1}), the combination bands involving two stretching and one bending CH motions (6500–7500 cm^{-1}), and the three quanta transitions involving the CH stretching motions (8000–9000 cm^{-1}). For these signals, as the temperature increases the absorbance of the spectrum decreases, in agreement with the reduction of the sample density.

As expected, the spectra of the two molecules differ where the contribution of the particular substituents (hydroxyl for DEHA and acetyl for DEAcA) is dominant. The first overtone of the hydroxyl group stretching lies at 7043 cm^{-1}, red-shifted by 54 cm^{-1} with respect to the signal recorded in the gas phase,[11] suggesting that in the liquid phase, the hydroxyl group is involved in a hydrogen bond. Accordingly, as the temperature increases and the hydrogen bonds start to break, the intensity of the peak increases and almost no frequency shift is observed. A similar behaviour has been reported for octanoic acid, where the OH stretching signal is strongly depleted at low temperatures due to the formation of dimers involving the double hydrogen bond binding between the carboxyl groups.[23] The hydroxyl stretching motion is also involved in the binary combination transition responsible for the broad peak at 4812 cm^{-1}, together with NOH bending motion. As it can be seen in the inset of Figure 6, as the temperature increases a blue-shifted shoulder rises (4879 cm^{-1}).

As regards the acetyl group, theoretical calculations predict a doublet at 4735 and 4805 cm^{-1} due to the binary combinations of the carbonyl stretching and the symmetric and asymmetric methyl stretching motions, respectively. In the same region, a strong peak centred at 4752 cm^{-1} and a blue-shifted shoulder (4788 cm^{-1}) are observed that can be associated with the acetyl. Accordingly, a doublet is found in the gas phase spectrum of acetaldehyde at about 4740 cm^{-1} and 4770 cm^{-1}.[24] The second overtone of the carbonyl stretching is found at 5238 cm^{-1}, 94 cm^{-1} red-shifted with respect to the theoretical value. Using a simplified model, which neglects the coupling between normal modes and considers the anharmonicity up to quadratic terms, the energy of a given vibrational normal mode is:[25]

$$G(n) = \tilde{\omega} \cdot \left(n + \frac{1}{2}\right) + \tilde{\omega} \cdot \chi \cdot \left(n + \frac{1}{2}\right)^2 \quad (3)$$

where $\tilde{\omega}$ is the harmonic wavenumber and $\tilde{\omega} \cdot \chi$ is the anharmonicity constant. Therefore the expression for the fundamental and overtone transitions wavenumbers is:

$$\tilde{\nu}_{n-0} = G(n) - G(0) = \tilde{\omega} \cdot n + \tilde{\omega} \cdot \chi \cdot (n^2 + n) \quad (4)$$

The anharmonicity constants computed from $(\tilde{\upsilon}_{02}/2 - \tilde{\upsilon}_{01})$ and $(\nu_{02}/2 - \nu_{01}/2)$ are -4 cm^{-1} and -10 cm^{-1}, respectively, which are equal to values obtained for acetaldehyde in solution at 295 K.[24] In order to obtain more reliable values, the least squares fitting was employed to reproduce the observed frequencies, resulting in a harmonic wavenumber $\tilde{\omega} =$ 1780 cm^{-1} and anharmonicity constant $\tilde{\omega} \cdot \chi = -8.4$ cm^{-1}. According to this model, the third C=O overtone is predicted at 6952 cm^{-1}, where some signal is present. Finally, we remark

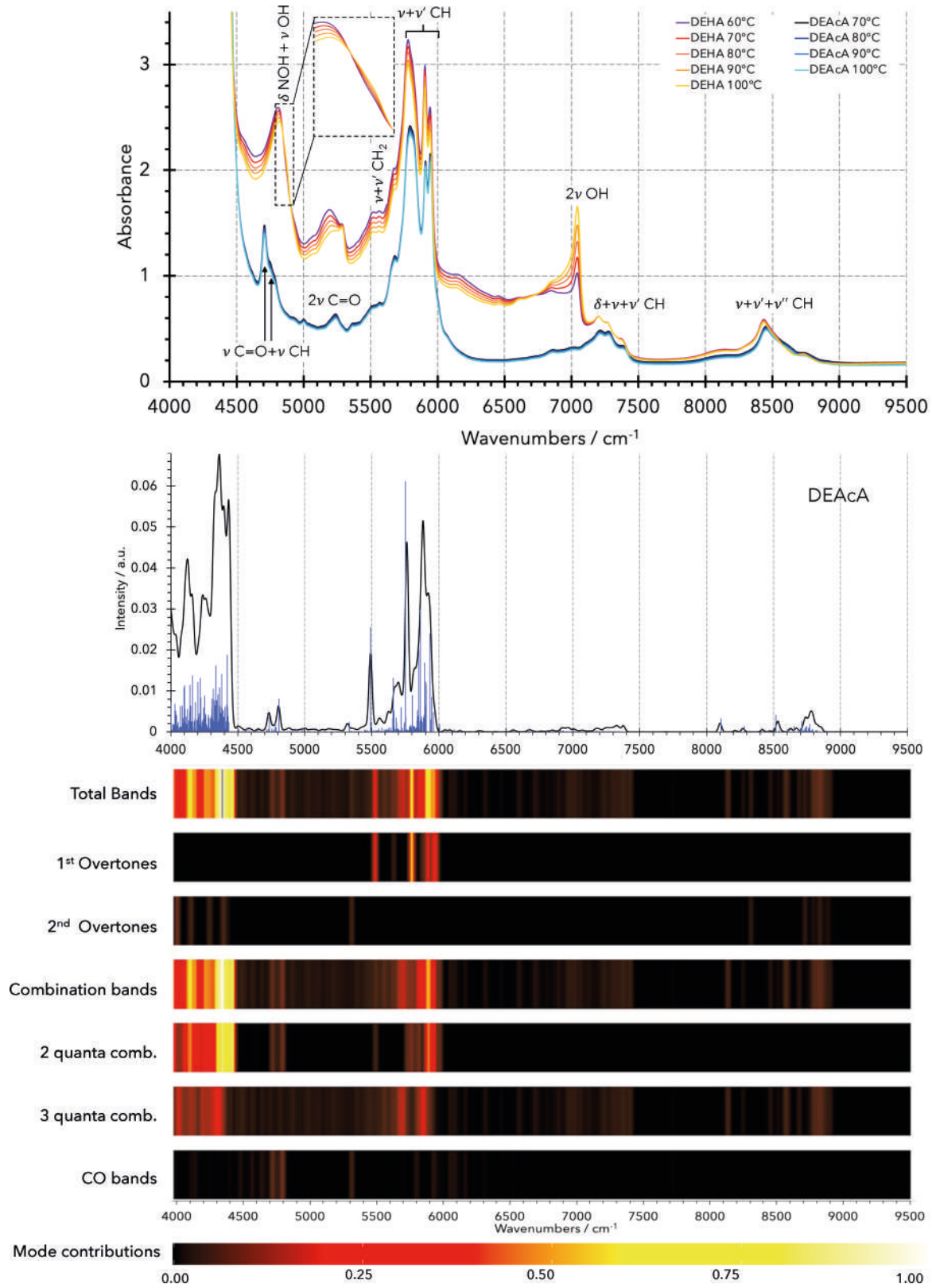

Figure 6. Top panel: Experimental NIR spectra of liquid DEHA and DEAcA recorded at different working temperatures. Middle panel: simulated (DFT) NIR spectrum of aaAs-DEAcA. Bottom panel: Heatmap bands of first and second overtones, combination bands split into binary and ternary combinations and carbonyl-related signals of DEAcA.

that the DEHA's features in the 5100–5400 cm^{-1} spectral region, are absent in the gas phase spectrum,[11] suggesting that they are related to the liquid phase.

Conclusions

The synthesis of DEAcA via acylation of DEHA was successfully achieved obtaining a high-purity product (98% yield) as confirmed by GC/EI-MS and NMR spectroscopy. Thermal stability assessment via DSC revealed a highly exothermic autocatalytic phenomenon with a peak temperature of 457 K and released energy of 174 $kJ\,mol^{-1}$, probably due to a decarboxylation reaction. DFT calculations corroborated experimental findings, emphasizing the need for cautious handling and storage of DEAcA.

The systematic theoretical exploration of the torsional degrees of freedom of DEAcA led to the identification of 25 non-equivalent local minima in the conformational space, allowing us to determine two general rules of thumb on their stability in the isolated phase: (*i*) the preferred arrangement of the alkyl frame (CCNCC) is all *anti*, as already found for DEHA;[11] (*ii*) the most stable conformers have the carbonyl group bond facing the nitrogen lone pair, leading to a wide region with negative electrostatic potential.

The main features of the vibrational spectra of DEHA and DEAcA in both the MIR and NIR regions have been disentangled with the support of DFT simulations, which satisfactorily reproduce the experimental data. The acetyl group's prominent features distinguished DEAcA from its counterparts, while the nitrogen-oxygen stretching revealed characteristic shifts upon acetylation. In particular, the first and second overtones of the C=O stretching have been observed allowing us to model its potential energy function. Moreover, analysis of bending and torsion modes facilitated conformational characterization. NIR spectroscopy, elucidated vibrational transitions and molecular interactions. Binary and ternary combination bands, alongside overtones, contribute to the spectral complexity with distinct features attributable to the functional groups. Temperature-dependent studies underscored the influence of intermolecular interactions, particularly evident in the behaviour of the hydroxyl group.

The presented comparative study on DEHA and DEAcA, combined with quantum mechanical simulations illustrates the interplay between molecular structure and spectroscopic vibrational properties signatures, providing new data on relatively understudied systems such as the N–O compounds.

Experimental

Synthesis of DEAcA (CAS 1842–68-8)

An oven-dried round bottom flask equipped with a magnetic stir bar and addition funnel was charged with DEHA (CAS 3710–84-7, 0.91 g, 10 mmol), triethylamine (CAS 121–44-8, 1.02 g, 10 mmol), and anhydrous dichloromethane (CAS 75–09-2, 20 ml). The addition funnel was charged with acetyl chloride (CAS 75–36-5, 0.80 g, 10 mmol) in anhydrous dichloromethane (10 ml) and the solution was added dropwise over 10 minutes at room temperature. The reaction mixture was stirred at room temperature for an additional 30 minutes. Then it was diluted with water (25 ml) and the organic layer was separated, washed with water (25 ml), and dried over sodium sulfate (CAS 7757–82-6). The solvent was removed under reduced pressure to afford a yellowish oil (1.45 g, 98% yield). The product was stored at 253 K under anhydrous conditions. GC/EI-MS mass peaks: 131 (main), 89 (main-acetyl + H), 74 (main-2×ethyl + H), 60 (*O*-acetyl + H), 43 (acetyl), 29 (ethyl), 15 (methyl). ^{1}H-NMR (400 MHz, $CDCl_3$: $\delta = 1.01$ (triplet, $J = 8.0$ Hz, $C\underline{H}_3CH_2N$), 1.75 (singlet, $C\underline{H}_3C{=}O$), 2.79 (quartet, $J = 8.0$ Hz, $CH_3C\underline{H}_2N$) ppm. ^{13}C-NMR (400 MHz, $CDCl_3$): $\delta = 12.38$ ($\underline{C}H_3CH_2N$), 19.82 ($\underline{C}H_3C{=}O$), 53.81 ($CH_3\underline{C}H_2N$), 171.08 ($CH_3\underline{C}{=}O$) ppm. The recorded spectra are available in the Supporting Information.

Characterization

Nuclear magnetic resonance spectra were collected on a Bruker 400 MHz spectrometer with TOPSPIN ver.4.1.1 software (US console AV400 Neo, Phrobe DUAL 400sB C–H-D-05). Gas-chromatography electron ionization mass spectrometry measurements were performed on an Agilent HRGC HP 6890 spectrometer equipped with MSD HP5373G detector. The differential scanning calorimeter 821e Mettler-Toledo was employed with Stare SW 16.20 software. MIR spectra were measured on a FT-IR Bruker Alpha spectrometer in attenuated total reflectance (ATR) mode. Measurements were performed in the 400–4000 cm^{-1} spectral range at a resolution of 4 cm^{-1}, using 16 scans per average and a zero filling factor 2, resulting in an interpolated data spacing of 2 cm^{-1}. NIR spectra were measured with a Bruker FT-NIR Spectrometer MPA II operating in absorbance mode and controlled by the manufacturer's Opus 8.1 software. Spectral measurements were performed in the 4000–10000 cm^{-1} spectral range at a resolution of 4 cm^{-1}, using a zero filling factor 2, resulting in an interpolated data spacing of 2 cm^{-1}. The Blackman-Harris 3-term apodization function was applied and 128 scans were accumulated. The provided experimental setup entails measuring the properties of two neat liquids, DEAcA and DEHA, across temperature ranges of 358.15 K to 388.15 K and 348.15 K to 388.15 K, respectively. This is done in increments of 10 K using a built-in sample temperature control module of the instrument and employing compatible glass vials with an 8 mm diameter for containment. The air background was subtracted and no additional spectral pretreatment was necessary.

Computations

Quantum mechanical calculations were performed using the GAUSSIAN16®software package (G16, Rev. A.03[1]). Local minima, harmonic and anharmonic vibrational frequencies were evaluated by density functional theory (DFT). The valence triple-ζ quality Karlsruhe polarised type basis set (Def2-TZVP)[26] was used in combination with the Becke-three-parameters Lee-Yang-Parr hybrid density functional theory (B3LYP)[27,28] corrected by the D3 version of Grimme's empirical dispersion with Becke-Johnson damping, D3(BJ).[29,30] The frequencies and absorption intensities of the two and three-quanta vibrational transitions were evaluated via the second-order vibrational perturbation theory (GPT2)[31,32] using a superfine grid for numerical integrations and a reduced-dimensionality scheme where the large amplitude motions ($\tilde{\nu} < 630\ cm^{-1}$) were not active. Since the anharmonic frequencies are sensitive to the ground state geometry,[22] tight convergence criteria of the molecular optimization protocol were

[1] Gaussian is a registered trademark of Gaussian, Inc. 340 Quinnipiac St. Bldg. 40 Wallingford, CT 06492 USA.

employed. IR and NIR spectra were simulated convoluting each peak with a Gaussian broadening function with $\sigma = 3.4\ cm^{-1}$ (FWHM 8 cm^{-1}) and $\sigma = 12\ cm^{-1}$ (FWHM 28.3 cm^{-1}), respectively. The potential energy distribution (PED) analysis of the vibrational normal modes was performed via VEDA4 program.[33] Additional geometry optimizations and harmonic frequency calculations were performed on selected structures at the following levels of calculations: M06-2X[34]/Def2-TZVP, MP2[35]/Def2-TZVP, B3LYP-D3(BJ)/aug-cc-pVTZ[36], M06-2X/aug-cc-pVTZ and MP2/aug-cc-pVTZ.

Acknowledgements

We acknowledge the CINECA award under the ISCRA initiative, for the availability of high-performance computing resources and support. This research is supported by the Italian Space Agency (project HELENA, award n. 2023-9-U.0, CUP-F33C23000310006) and the Emilia-Romagna Region (POR FESR 21-27, project SMAL-SAT, award n. PG/2023/308391, CUP-J47G22000720003). Open Access publishing facilitated by Università degli Studi di Bologna, as part of the Wiley - CRUI-CARE agreement.

Conflict of Interests

The authors declare no conflict of interest.

Data Availability Statement

The data supporting this study's findings are available in this article's supplementary material.

Keywords: Oxyamine · Synthesis · Quantum Mechanical Modeling · Infrared Spectroscopy · Near-Infrared Spectroscopy · Conformational Space

[1] Y. Ozaki, C. Huck, Near-Infrared Spectroscopy: Theory, Spectra Analysis, Instrumentation, and Applications, Springer Singapore, Singapore **2021**.
[2] K. B. Bec, J. Grabska, C. W. Huck, *Spectrochim. Acta Part A* **2021**, *254*, 119625.
[3] H. R. Lamontagne, B. H. Lessard, *ACS Appl. Polym. Mater.* **2020**, *2*, 5327.
[4] A. Vebr, M. Dallegre, L. Autissier, C. Drappier, K. Le Jeune, D. Gigmes, A. Kermagoret, *Polym. Chem.* **2022**, *13*, 3275.
[5] J. L. Hodgson, M. L. Coote, *Macromolecules* **2010**, *43*, 4573.
[6] T. Reyser, T. H. To, C. Egwu, L. Paloque, M. Nguyen, A. Hamouy, J.-L. Stigliani, C. Bijani, J.-M. Augereau, J.-P. Joly, J. Portela, J. Havot, S. R. A. Marque, J. Boissier, A. Robert, F. Benoit-Vical, G. Audran, *Molecules* **2020**, *25*.
[7] G. Audran, S. R. A. Marque, P. Mellet, *Acc. Chem. Res.* **2020**, *53*, 2828.
[8] S. Munneke, J. R. C. Prevost, G. F. Painter, B. L. Stocker, M. S. M. Timmer, *Org. Lett.* **2015**, *17*, 624.
[9] X.-G. Liu, H. Gao, S.-S. Zhang, Q. Li, H. Wang, *ACS Catal.* **2017**, *7*, 5078.
[10] B. Bouvet, S. Sene, G. Felix, J. Havot, G. Audran, S. R. A. Marque, J. Larionova, Y. Guari, *Nanoscale* **2023**, *15*, 144.
[11] G. Salvitti, E. Pizzano, F. Baroncelli, S. Melandri, L. Evangelisti, F. Negri, M. Coreno, K. C. Prince, A. Ciavardini, H. Sa'adeh, M. Pori, M. Mazzacurati, A. Maris, *Spectrochim. Acta Part A Mol. Biomol. Spectrosc.* **2022**, *281*, 121555.
[12] F. Baroncelli, G. Panizzi, L. Evangelisti, S. Melandri, A. Maris, *J. Mol. Spectrosc.* **2023**, *392*, 111759.
[13] G. Salvitti, F. Baroncelli, C. Nicotri, L. Evangelisti, S. Melandri, A. Maris, *Molecules* **2022**, *27*, 8190.
[14] G. Zinner, *Chem. Ber.* **1958**, *91*, 302.
[15] R. Huisgen, F. Bayerlein, *Justus Liebigs Ann. Chem.* **1960**, *630*, 138.
[16] C. L. Perrin, J. D. Thoburn, S. Elsheimer, *J. Org. Chem.* **1991**, *56*, 7034.
[17] A. M. Berman, J. S. Johnson, *J. Am. Chem. Soc.* **2004**, *126*, 5680.
[18] P. Linstrom, W. Mallard (Editors), NIST Chemistry WebBook, NIST Standard Reference Database Number 69, National Institute of Standards and Technology, Gaithersburg MD, 20899 Accessed 2024-04-01.
[19] O. Exner, B. Kakac, *Collect. Czech. Chem. Commun.* **1960**, *25*, 2530.
[20] W. George, T. Houston, W. Harris, *Spectrochim. Acta Part A Mol. Spectrosc.* **1974**, *30*, 1035.
[21] R. E. Nightingale, E. L. Wagner, *J. Chem. Phys.* **1954**, *22*, 203.
[22] K. Bec, Y. Futami, M. J. Wójcik, Y. Ozaki, *Phys. Chem. Chem. Phys.* **2016**, *18*, 13666.
[23] M. A. Czarnecki, Y. Liu, Y. Ozaki, M. Suzuki, M. Iwahashi, *Appl. Spectrosc.* **1993**, *47*, 2162.
[24] G. Lucazeau, C. Sandorfy, *Can. J. Chem.* **1970**, *48*, 3694.
[25] G. Herzberg, Molecular Spectra and Molecular Structure: Infrared and Raman spectra of polyatomic molecules, Molecular Spectra and Molecular Structure, R. E. Krieger Publishing Company **1991**.
[26] F. Weigend, R. Ahlrichs, *Phys. Chem. Chem. Phys.* **2005**, *7*, 3297.
[27] A. D. Becke, *J. Chem. Phys.* **1993**, *98*, 5648.
[28] C. Lee, W. Yang, R. G. Parr, *Phys. Rev. B* **1988**, *37*, 785.
[29] S. Grimme, J. Antony, S. Ehrlich, H. Krieg, *J. Chem. Phys.* **2010**, *132*, 154104.
[30] S. Grimme, S. Ehrlich, L. Goerigk, *J Comp. Chem.* **2011**, *32*, 1456.
[31] V. Barone, *J. Chem. Phys.* **2005**, *122*, 014108.
[32] J. Bloino, V. Barone, *J. Chem. Phys.* **2012**, *136*, 124108.
[33] M. H. Jamróz, *Spectrochim. Acta Part A* **2013**, *114*, 220.
[34] Y. Zhao, D. G. Truhlar, *Theor. Chem. Acc.* **2008**, *120*, 215.
[35] C. Müller, M. Plesset, *Phys. Rev.* **1934**, *46*, 618.
[36] T. Dunning Jr., *J. Chem. Phys.* **1989**, *90*, 1007.

Manuscript received: February 29, 2024
Revised manuscript received: April 10, 2024
Accepted manuscript online: July 4, 2024
Version of record online: September 9, 2024